Contents lists available at ScienceDirect

Analytica Chimica Acta

journal homepage: http://ees.elsevier.com

The molecular bases of chiral recognition in 2-(benzylsulfinyl)benzamide enantioseparation

Paola Peluso [a,*], Bezhan Chankvetadze [b,**]

[a] Istituto di Chimica Biomolecolare ICB-CNR, Sede Secondaria di Sassari, Traversa La Crucca 3, Regione Baldinca, Li Punti, 07100 Sassari, Italy
[b] Institute of Physical and Analytical Chemistry, School of Exact and Natural Sciences, Tbilisi State University, Chavchavadze Ave 3, 0179 Tbilisi, Georgia

ARTICLE INFO

Article history:
Received 19 September 2020
Received in revised form 19 October 2020
Accepted 23 October 2020
Available online xxx

Keywords
Cellulose-based chiral stationary phases
Chiral sulfoxides
Electrostatic potential
Enantioseparation
High-performance liquid chromatography

ABSTRACT

Liquid-phase chromatography on chiral stationary phase is still the most popular and versatile technique to separate enantiomers, which is based on the ability of a chiral selector (CS) to recognize the enantiomers of a chiral compound in a solvating medium. The knowledge of the molecular bases of the enantiodiscrimination process is a basic requirement to approach rationally the enantioseparation task. Indeed, analyte, CS, and mobile phase (MP) being the pivotal components of the chromatographic system, their properties, functions and mutual noncovalent interactions determine the enantioseparation outcome. In the last few decades, focused computational methods and techniques have been integrating experimental data and applying for the comprehension of the enantiorecognition phenomenon at molecular level. In this context, for understanding of molecular mechanisms of chiral recognition in separation of enantiomers, we propose a computational procedure based on conformational and electrostatic potential (*V*) analysis of both analyte and selector. First, low-energy conformers of the analyte were identified by conformational search, which occurring potentially on the selector surface. Then, local electron charge density of specific molecular regions of the interacting partners were inspected in terms of calculated *V*. This approach was used to explore at molecular level the enantioseparation mechanism of 2-(benzylsulfinyl)benzamide on cellulose-based CSs. By correlating calculated properties with experimental chromatographic parameters available in the literature, the structural landscape of the analyte and CSs in the enantiodiscrimination event and the differences between potential competing sites were profiled. A conformational transition of analyte structure on the CS surface was found to originate the exceptional enantioseparation of the 2-(benzylsulfinyl)benzamide ($\alpha > 100$). Importantly, the proposed computational analysis provides a rationale of why and how the analytical separation occurs.

1. Introduction

The interest of science and global market in pure enantiomers originates in the ability of endogenous chiral molecules to recognize and discriminate enantiomers, with important consequences at biological and biochemical levels [1,2]. Because two enantiomers possess the same chemo-physical properties in isotropic medium, their separation is generally more demanding compared to achiral separations. Nowadays, high-performance liquid chromatography on polysaccharide phenylcarbamate-based chiral stationary phases (CSPs) still remains the mostly used technique to separate enantiomers [3,4]. The pivotal components of this chromatographic system are chiral analyte, the polymeric chiral selector (CS) and mobile phase (MP). The enantiomers adsorb on the chiral surface forming transient diastereomeric complexes which are energetically and kinetically distinguishable. The overall process consists of consecutive adsorption-desorption steps which lead to the separation of enantiomers due to incremental differences between their retention times.

Understanding enantioseparation at molecular level is a basic requirement for approaching rationally the enantioseparation task at chromatographic level. Actually, unravelling the molecular bases of recognition mechanisms remains an open issue for polysaccharide-based CSs due to the level of intricacy of their structure [5,6]. The basic structural components of amylose and cellulose phenylcarbamates are the backbone and the aromatic carbamate side chains (SCs) (Fig. 1a). These molecular tentacles are characterized by distinctive steric and electronic properties which can be tuned by changing type and position of the substituents onto the terminal aromatic ring. Both backbone and SCs contribute to form chiral cavities which can match shape and size of the analyte, so favouring its stereoselective fit through noncovalent interactions occurring at the surface of the CS [4,6].

* Corresponding author. Istituto di Chimica Biomolecolare ICB-CNR Sede secondaria di Sassari Traversa La Crucca 3 Regione Baldinca 07100 Sassari, Li Punti Italy.
** Corresponding author.
E-mail addresses: paola.peluso@cnr.it (P. Peluso); jpba_bezhan@yahoo.com (B. Chankvetadze)

https://doi.org/10.1016/j.aca.2020.10.050
0003-2670/

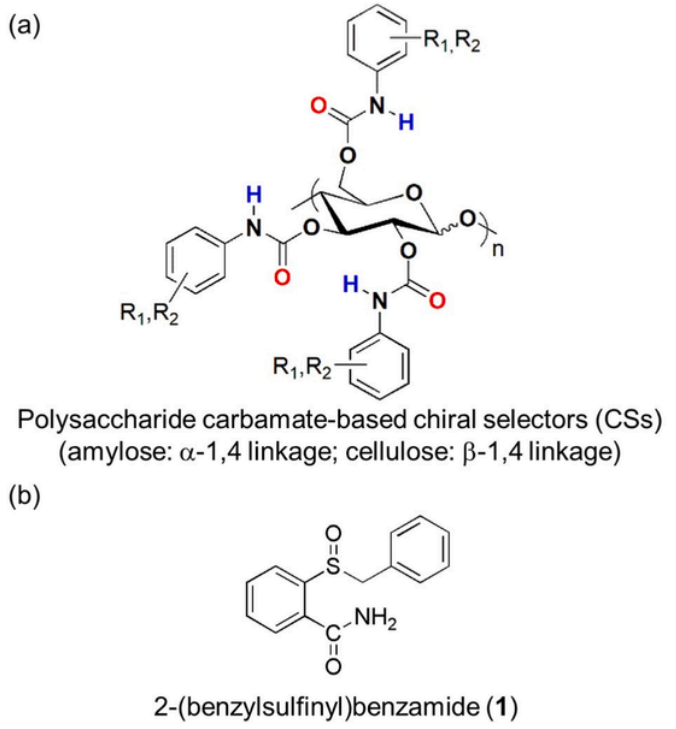

Fig. 1. General structures of (a) polysaccharide carbamate-based chiral selectors (CSs), and (b) chiral sulfoxide **1**.

In the last decades, the growing interplay between experimental and theoretical approaches has allowed for exploring intermolecular forces underlying selector-analyte association [7,8]. In general, computational approaches to explore enantiodiscrimination at molecular level can be performed by calculating either features and energies of enantiomer-CS complexes, or the molecular properties (shape, geometry and electronic distribution) of both analyte and selector in their unperturbed state. In this case, the scope of the computational analysis is to identify chemical and electronic features which may determine noncovalent interactions underlying enantioselective adsorption and enantiomer separation.

Along with noncovalent interactions, conformational features of analyte and CS as well as the possibility of mutual analyte-CS conformational adjustments may impact the recognition process and contribute to enhance the enantioseparation extent [9–11].

Enantioseparations with exceptionally high selectivity are very useful as benchmark discrimination processes to gain information on the molecular bases of very efficient recognition mechanisms which produce high-selectivity results at macroscopic level [12–15]. In this regard, the enantioseparation of 2-(benzylsulfinyl)benzamide (**1**) (Fig. 1b) represents an intriguing case study. Whereas simple chiral sulfoxides such as **2**–**4** (Fig. 2), and other derivatives of pharmaceutical interest, usually show rather standard selectivity factors on polysaccharide-based CSs [16–23], exceptional selectivity (α = 112, enantiomer elution order (EEO) = *R*-(+)-*S*-(−)) was observed for the enantioseparation of **1** on coated cellulose *tris*(3,5-dichlorophenylcarbamate) (CD-CPC) (**CS1**) (Table 1) with 2-propanol as MP [12,24]. In particular, both retention factors (*k*) and α values were found to increase in the order methanol < ethanol < 2-propanol. Later, Cirilli and co-authors also observed high selectivity values (MP, 2-propanol: α = 43; MP, *n*-hexane/2-propanol 80:20: α = 150) for the enantioseparation of **1** (EEO *R*–*S*) on the immobilized CDCPC [25]. Higher enantioselectivity (α = 85, EEO *R*–*S*) was also reported by the same group for the enantioseparation of 2-(pentylsulfinyl)benzamide **5** compared to the analogs **6**–**9** on the immobilized CDCPC with *n*-hexane/2-propanol 80:20 as MP [26]. In the last few years, Chankvetadze and co-authors have intensively investigated the enantioseparation of **1** and other related chiral sulfoxides (**10**–**22**) (Fig. 2) on the series of cellulose-based **CS1**-**CS17** (Table 1) with *n*-hexane-based mixtures, polar organic solvents and aqueous-organic mixture as MPs [12,27–32]. In particular, for **1** high enantioselectivity (α = 202.6) was observed on cellulose *tris*(4-chloro-3-methylphenylcarbamate) (**CS16**) with *n*-hexane/2-propanol 70:30 as

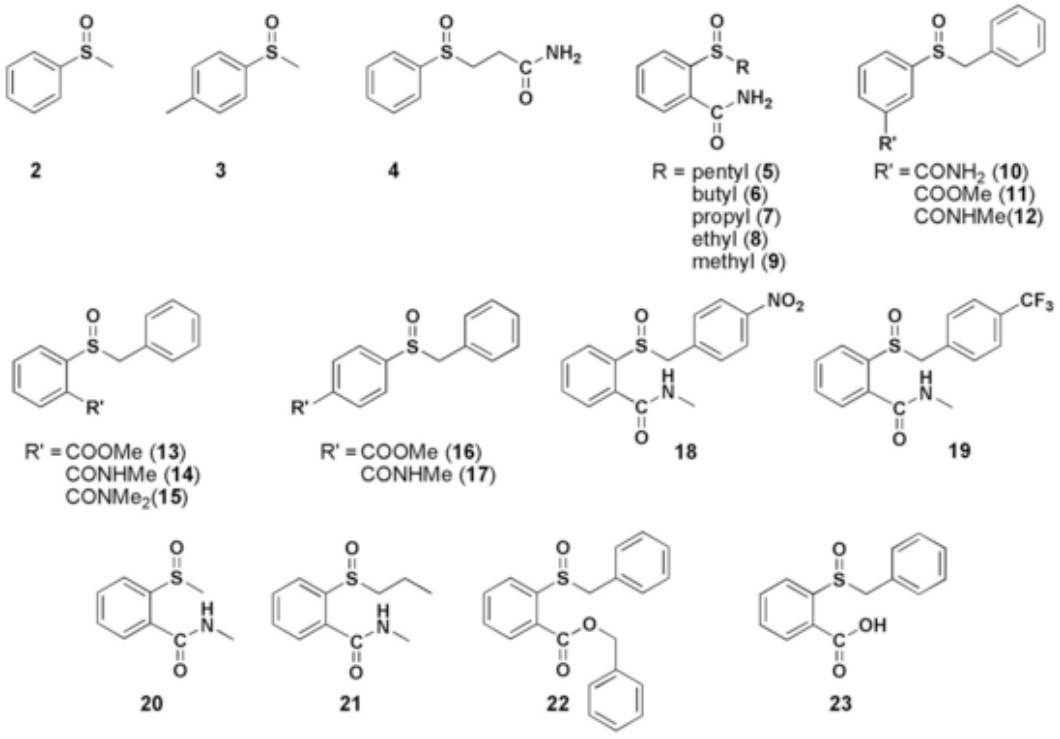

Fig. 2. Structures of chiral sulfoxides **2**–**23**.

Table 1
Distinctive substituents of cellulose-based CS1-CS17 and SC1-SC17 models.

CS	SC	R_1	R_2
CS1	**SC1**	3-Cl	5-Cl
CS2	**SC2**	3-Me	5-Me
CS3	**SC3**	2-Cl	H
CS4	**SC4**	3-Cl	H
CS5	**SC5**	4-Cl	H
CS6	**SC6**	2-Cl	3-Cl
CS7	**SC7**	2-Cl	4-Cl
CS8	**SC8**	2-Cl	5-Cl
CS9	**SC9**	2-Cl	6-Cl
CS10	**SC10**	3-Cl	4-Cl
CS11	**SC11**	2-Me	H
CS12	**SC12**	3-Me	H
CS13	**SC13**	4-Me	H
CS14	**SC14**	3-Me	4-Me
CS15	**SC15**	3-Cl	4-Me
CS16	**SC16**	3-Me	4-Cl
CS17	**SC17**	H	H

MP [27]. In 2017, the enantioseparation of **1** and related derivatives were studied on chlorinated polysaccharide CSs in supercritical fluid chromatography (SFC) by West and co-authors [33]. Very recently, Cavazzini observed an unusual convex-upward van Deemter curve for the second eluted enantiomer of **1** on **CS16**, whereas the first eluted enantiomer showed a more traditional convex-downward curve [34].

The studies performed so far evidenced that, for the enantioseparations of **1** and related derivatives on cellulose-based CSs, very high selectivity values are strictly dependent on the presence of pivotal features in both chiral sulfoxide and CS, namely the amidic NH_2 group and chlorine as substituent, respectively. It was shown that hydrogen bonds (HBs) play the dominant role for enantioseparations. In fact, any modifications which weaken HBs led to a dramatic drop of selectivity [12,25]. Nevertheless, the molecular bases of this enantioseparations remain unknown and the matter still presents some open issues: *i)* on most cellulose phenylcarbamate CSs, **1** shows exceptional retention of one enantiomer and minimal retention of the other enantiomer; *ii)* subtle structural modifications at any position of the lead scaffold impact selectivity in almost all cases; *iii)* moving the benzylsulfinyl substituent from position 2 (compound **1**) to position 3 (compound **10**) with respect to the amide group (Fig. 2), leads to a dramatic drop (or loss) of enantioseparation; *iv)* on most CSs, the first eluted enantiomer of **1** retains shorter than the first eluted enantiomer of **10**.

Over time, computational-aided studies on recognition mechanisms of polysaccharide-based CSPs towards chiral sulfoxides were reported [23,33,35,36]. Among them, only one recent article deals with the enantioseparation of **1** and related derivatives, determining the lowest energy conformers through conformational search performed with the MMFF94x force field and Born solvation [33].

Given this context, with the aim of unravelling the molecular origins of retention and enantioselectivity observed for **1** and related derivatives on cellulose-based CSs, chemical, electronic and conformational features of the interacting partners were computed, and their impact on enantioseparation was inspected. Low-energy conformers of **1** were identified through conformational search, and molecular properties and electrostatic potential (*V*) values were calculated for each conformer at density functional theory (DFT) level. In addition, the electronic properties of carbamate frameworks **SC1**-**SC17**, as models of the SC regions of cellulose-based **CS1**-**CS17**, were computed (Table 1). On this basis, the possible correlations between calculated properties and experimental retention and selectivity factors were explored. For this purpose, chromatographic parameters of reported enantioseparations were used as benchmark experimental data.

2. Computationals

The 3D structures of analytes and SCs were prepared by using the build function, and model kits and tools provided by Spartan' 10 Version 1.1.0 (Wavefunction Inc., Irvine, CA, USA) [37] for building and editing organic molecules. On this basis, molecules were generated and their structure refinement was performed by a MMFF procedure. Then, each structure was submitted to a conformational systematic search using the MMFF force field, spanning all shapes accessible to the molecule without regard to energy. After the elimination of duplicates and high-energy conformers, a set of energetically accessible conformers was selected. For each conformer, geometry optimization was performed in vacuum employing the DFT method with the B3LYP functional and the 6-31G* basis set, and finally the respective Boltzmann distribution (%) was constructed. In some cases, energies (given in kcal/mol) and Boltzmann distributions were also calculated in methanol as solvation environment. In this case, the SM8 solvation model [38,39] was applied. Computation of *V* values mapped on 0.002 au electron density isosurfaces (V_S) and related parameters (V_S maxima ($V_{S,max}$) and minima ($V_{S,min}$) values, given in kJ/mol, isosurface area [Å^2] and volume enclosed in the isosurface area [Å^3]) was performed and graphically generated by using Spartan' 10 (DFT/B3LYP/6-31G*). V_S isosurface colours towards red depict negative V_S values, while colours towards blue depict positive V_S values and colours in between (orange, yellow, green) depict intermediate values of V_S. Statgraphics Centurion XVIII (Statpoint Technologies, Inc., Warrenton, VA, USA) was used for all regression analyses.

3. Results and discussion

3.1. Calculation of electrostatic potential to inspect interaction sites

Given a molecule, the $V(\mathbf{r})$ at each point $\mathbf{r}$ in the surrounding space, is created by each nucleus (first positive term) and electron (second negative term) of the molecule and given by equation (1)

$$V(r)\cdot = \cdot \sum_A \frac{Z_A}{R_A - \mathbf{r}} - \int \frac{\rho(\mathbf{r})d\mathbf{r}'}{|\mathbf{r}' - \mathbf{r}|} \quad (1)$$

where Z_A is the charge on nucleus A located at R_A, and $\rho(\mathbf{r})$ is the electron density function [6,40]. Thus, the sign of *V* may be positive or negative depending on the dominant contribution, which is positive and negative from nuclei and electrons, respectively. *V* is a real physical property, and the evaluation of its variations on a molecular electron density isosurface accounts for the shape of the molecule which is the sum of geometry and electronic distribution. Therefore, by mapping *V* on electron density isosurfaces (V_S), the electron charge density on molecular regions involved in the noncovalent contacts may be evaluated, deriving V_S-based guidelines to predict and profile interaction patterns. In particular, regions with high (nucleophile, HB acceptors) and low (electrophile, HB donors) electron charge density can be identified by $V_{S,min}$ and $V_{S,max}$ values, respectively.

On this basis, in the last few years *V* analysis of analytes and polysaccharide-based CSs in their isolated state was advantageously used to rationalize noncovalent interaction patterns underlying enantiodiscrimination [41–43]. This approach relies on the concept that the enantioseparation is a phenomenon involving interactions at the surface between selector and analyte. V_S is not an anisotropic property, however the electron charge density distribution on specific regions of a chiral compound may produce anisotropic effects impacting analyte-selector complex formation. In this perspective, calculating V_S provides important information on the 3D-shape of the distinctive enantiophoric system (*the basic combination of the spatial structural features which are supposed to be responsible for chiral recognition* [44]) associated with the analyte structure.

Studying the interacting partners in their isolated state may be considered unsuitable to account for the dynamic feature of the enan-

tioseparation event. On the other hand, it is well acknowledged that the general features of noncovalent interactions may be well explained on the basis of their electrostatic nature [45]. In this regard, recently Clark proposed three levels of interaction for the analysis of weak intermolecular contacts [46]: (*i*) a first level containing classical electrostatic interactions (*permanent electrostatic interactions*) that can be evidenced by inspecting the unperturbed V_S of an isolated molecule [47], (*ii*) a second level improving the previous view by introducing the mutual polarization of interacting molecules (*induced electrostatic interactions*), and (*iii*) a third level including dispersion. The first level is based on the approximation of inspecting the interacting partners in their isolated state, thus mutual polarization and dispersion effects are not considered. However, electrostatic modelling at this level proved to be adequate in many cases, explaining binding energy, interaction geometry, and directional preference [6,48].

3.2. Comparative structural analysis of compounds *1*–*4*, and *22*

Sulfoxides **1**–**4** and **22** were selected in order to evaluate the impact of introducing the benzyl framework (**1**, **22**), $CONH_2$ (**1**, **4**) and COOR (**22**) groups, as distinctive substituents, on the conformational and electronic features of each structure, given the phenylsulfinyl unit as the common subunit. On this basis, low-energy conformers were calculated for compounds **1**–**4**, and **22**. One conformer was identified for the simple sulfoxides **2** and **3**, whereas seven conformers with Boltzmann distribution higher than 0.1% were found for compound **22** due to the greater number of rotatable bonds (Supplementary data, Fig. S1). For compound **4**, several conformers were found, which can be referred to two conformational patterns generated by the relative position of the amidic NH_2 group, which can be close to the sulfinyl oxygen, with formation of an intramolecular HB (S═O···H–N, conformer $\mathbf{4}_{HB}$) or far from it (conformer $\mathbf{4}_{freeNH2}$) (Fig. 3a). For **1**, four low-energy conformers were found (Fig. 3b). They originate from the relative orientation of the two phenyl rings (benzamide and benzyl frameworks) that can be close to each other (*bent conformer*) or away from each other (*linear conformer*) due to free rotation around the C–C and C–S bonds. For each of the two conformations, analogously to compound **4**, two additional conformers are generated by the relative position of the $CONH_2$ group, which can be close to the S═O group, with formation of an intramolecular HB ($\mathbf{1}_{HB\_bent}$ and $\mathbf{1}_{HB\_linear}$), or far from it ($\mathbf{1}_{freeNH2\_bent}$ and $\mathbf{1}_{freeNH2\_linear}$). The relative energies of all conformers were calculated in vacuum and are reported in Fig. 3. The zero value of energy was ascribed to the most stable conformer. The energy values may allow determination of the relative Boltzmann distribution (Supplementary data, Table S1). For each conformer, V_S isosurfaces and related parameters were calculated: $V_{s,min}$ associated with the electron charge density on sulfinyl oxygens (**1**–**4**, **22**), carbonyl oxygens (**1**, **4**, **22**), and phenyl rings (**1**–**4**, **22**), $V_{S,max}$ on the amidic hydrogen (**1**, **4**), isosurface area, polar area, nonpolar area, volume enclosed in the isosurface, dipole moment, and log P (see Supplementary data, Table S2). For conformers of compound **22**, the electron charge density on the carbonyl oxygen appeared lower (-141.2 kJ/mol $\leq V_{S,min} \leq -128.4$ kJ/mol) compared to the sulfinyl oxygen (-227.5 kJ/mol $\leq V_{S,min} \leq -210.0$ kJ/mol) due to partial overlapping of the aromatic rings which surround the carbonyl moiety and make it rather inaccessible as a HB acceptor. For compounds **1** and **4**, it was observed that the enantiophore system changes as the molecular conformational pattern. Indeed, conformers showing a free NH_2 group present higher electron charge density on the sulfinyl oxygen compared to the carbonyl oxygen ($V_{S,min}$ (S═O) ranging from -229.4 to -207.1 kJ/mol < $V_{S,min}$ (C═O) ranging from -186.6 to -151.1 kJ/mol), with two more positive regions located on each amidic hydrogen ($V_{S,max}$ ranges from 195.3 to 241.0 kJ/mol). Differently, conformers which present the intramolecular S═O···H–N contact (with distances ranging from 1.77 to 1.88 Å) are characterized by higher electron charge density on the carbonyl oxygen compared to the sulfinyl oxygen ($V_{S,min}$ (C═O) ranging from -217.7 to -192.1 kJ/mol < $V_{S,min}$ (S═O) ranging from -182.6 to -167.1 kJ/mol). Indeed, the sulfinyl oxygen being involved as HB acceptor, its electron charge density decreases and, consequently, the associated $V_{S,min}$ is less negative. On the other hand, in this case a moderately positive $V_{S,max}$ value is detectable on one amidic hydrogen (ranging from 153.0 to 168.8 kJ/mol), the other one being involved in the intramolecular HB. It is worth mentioning that less negative $V_{S,min}$ on the sulfinyl oxygen (-180.8, -182.6 kJ/mol) and the lower $V_{S,max}$ values (166.8, 168.2 kJ/mol) on the amidic hydrogen were calculated for the conformers $\mathbf{1}_{HB}$. Otherwise, the most negative $V_{S,min}$ on the sulfinyl oxygen (-229.4 kJ/mol) as well as the highest $V_{S,max}$ value on the amidic hydrogen (241.0 kJ/mol) were found in the conformer $\mathbf{1}_{freeNH2\_linear}$. This calculated structure matches the structure of (*S*)-**1** crystallized from a methanol/pentane solution and reported by Cirilli and co-authors [25] (Supplementary data, Fig. S2).

3.2.1. Correlation between computational and experimental chromatographic data

Comparative enantioseparations of chiral sulfoxides **1**–**4**, and **22** on **CS1** (coated CSP) were reported by using polar organic MPs [12]. In this series of enantioseparations, selectivity values increased following the order **2**, **3** < **4** < **22** « **1** (Supplementary data, Table S3). Interestingly, **1** showed the lowest and the highest retention values for the first (*R*) and the second (*S*) eluted enantiomer, respectively. In particular, with 2-propanol 100% (favouring HB formation) as MP, a $\Delta\alpha = 109.7$ could be observed moving from **2** to **1**. Therefore, with the aim to explore the structural reasons of this unusual chromatographic behaviour, the possible correlation between calculated molecular properties (conformational features and electron charge density distribution) in vacuum and reported retention and selectivity factors in 2-propanol was explored by fitting a simple linear regression model to describe the relationship between ln $k_{1,2}$ (dependent variables) and computed properties as independent variables. It is worth mentioning that in calculations performed in the vacuum, the solvent effect was not considered. The computation of properties in the vacuum is a quite realistic situation when nonpolar hydrocarbon-based eluents or 2-propanol (favouring HB formation) are used. The final results were obtained by searching the set of computed properties producing the best r^2 and P-value (<0.05), spanning all values related to low-energy conformers of **2**, **3**, seven conformers of **22** (see Supplementary data, Fig. S1, Table S2), conformers $\mathbf{4}_{HB}$ and $\mathbf{4}_{freeNH2}$, and conformers $\mathbf{1}_{HB\_bent}$, $\mathbf{1}_{HB\_linear}$, $\mathbf{1}_{freeNH2\_bent}$ and $\mathbf{1}_{freeNH2\_linear}$ (Fig. 3). No clear and statistically significant correlation was obtained between ln $k_{1,2}$ and $V_{S,min}$ on the aromatic rings, isosurface area, polar area, volume, and log P, as independent variables. The lack of a correlation representing all five selected compounds means that the calculated properties do not impact enantioseparations in the same sense or with the same relevance in all cases. However, this observation does not rule out the possibility that the mentioned properties influence the enantioseparation of a specific compound in a distinctive manner. Otherwise, the best results were found with a series of $V_{S,min}$ values associated with the HB acceptor sites (S═O and/or C═O), as independent variables (Fig. 4), this correlation showing the dominant role of the HBs between acceptors of the analytes and donors (amidic hydrogens) of the CSs. For **4** the best values of $V_{S,min}$ is associated with the electron charge density on the carbonyl oxygen of conformer $\mathbf{4}_{HB}$, whereas for the other compounds the best values are associated with the sulfinyl oxygens. In particular, associating each value of the best $V_{S,min}$ data set to the corresponding conformer allowed for getting information on the preferred conformational features of the analyte on the CS surface. For **1**, two different best $V_{S,min}$ values associated with the sulfinyl oxygens were found for each regression lines ln $k_1 = f(V_{S,min})$ and ln $k_2 = f(V_{S,min})$, which correspond to two different conformers, the $\mathbf{1}_{HB\_linear}$ for retention of the first eluted enantiomer and $\mathbf{1}_{freeNH2\_linear}$ for retention of the second eluted enantiomer. On the other hand, the energy differences between calculated conformers being rather low, conformational transition between

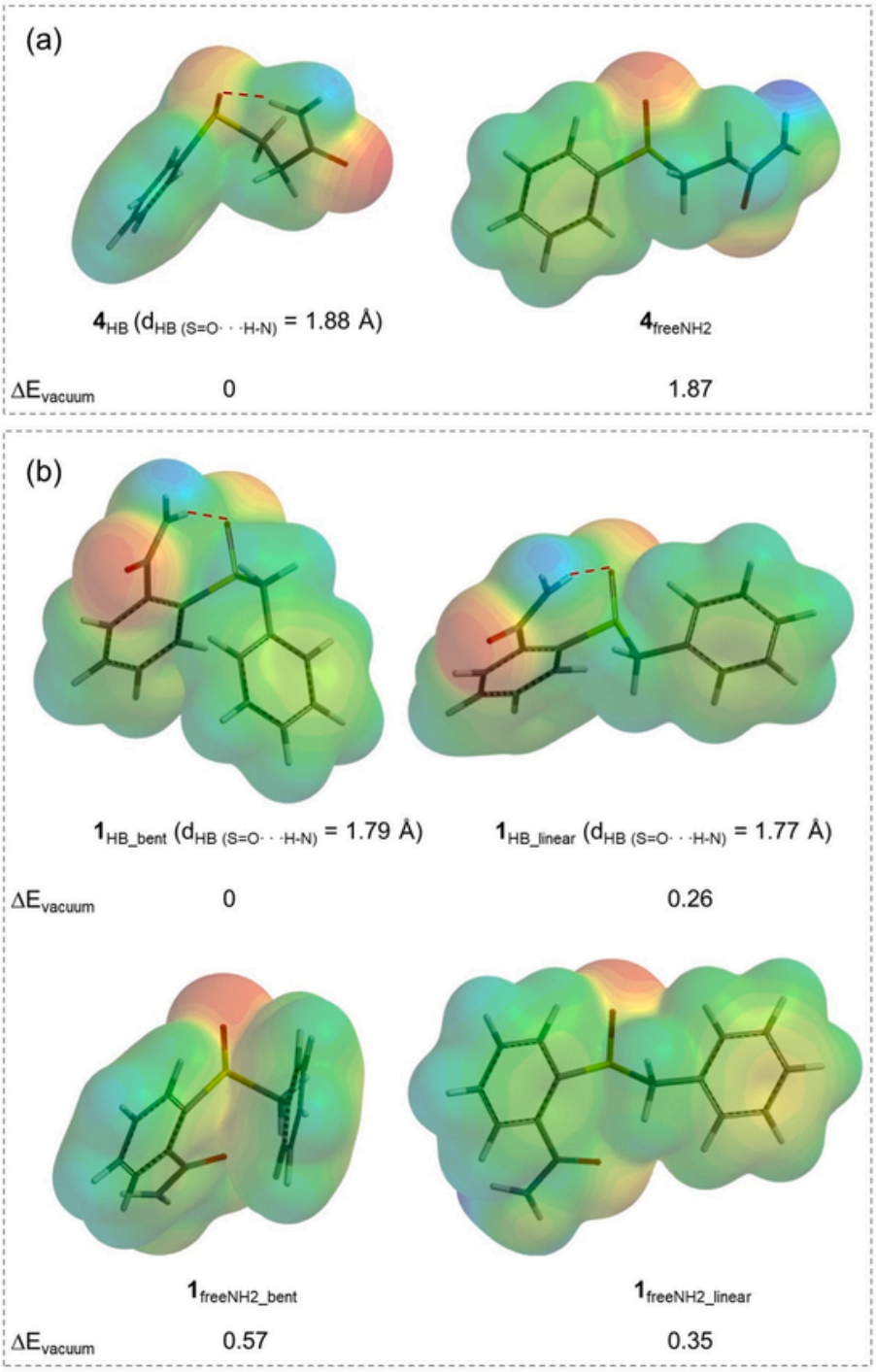

Fig. 3. V_S representation on electron density isosurfaces of low-energy conformers calculated for (a) **4** and (b) **1**. Relative energy values are reported [kcal/mol]. Colours towards red depict negative V_S, while colours towards blue depict positive V_S, and colours in between (orange, yellow, green) depict intermediate values. (For interpretation of the references to colour in this figure legend, the reader is referred to the Web version of this article.)

conformers appears to be likely on the CS surface. Coherently with the trend in terms of retention of first (k_1 = 0.99) and second eluted enantiomer (k_2 = 109.8), for **1** the $V_{S,min}$ (−182.6 kJ/mol) in the line ln $k_1 = f$ ($V_{S,min}$) (red line) is the less negative value in series **1**–**4** and **22**, belonging to the conformer $\mathbf{1}_{HB\_linear}$, whereas the opposite occurs for the $V_{S,min}$ (−229.4 kJ/mol) (conformer $\mathbf{1}_{freeNH2\_linear}$) of the line ln $k_2 = f$ ($V_{S,min}$) (blue line). Therefore, on the basis of this *conformationally-driven model*, the exceptional selectivity of **1** on **CS1** with 2-propanol (or with *n*-hexane-based mixtures) emerges from the discrimination of the two enantiomers as two distinctive conformational forms which represent two different enantiophoric systems eluting along the surface of the CS. The first eluted enantiomer (*R*)-**1** shows less conformational freedom being constrained by an intramolecular HB which reduces its ability to exert intermolecular contacts with the CS. Otherwise, the second eluted enantiomer (*S*)-**1** presents no intramolecular HB, thus it has conformational freedom and enhanced ability to interact with CS surface. In this regard, it is worth mentioning that very recently, in a case study on the enantioseparation of carnosine enantiomers on Teicoplanin A2-2-based CSP (EEO *S*-*R*), Carotti and co-authors found that (*S*)-carnosine establishes intramolecular contacts be-

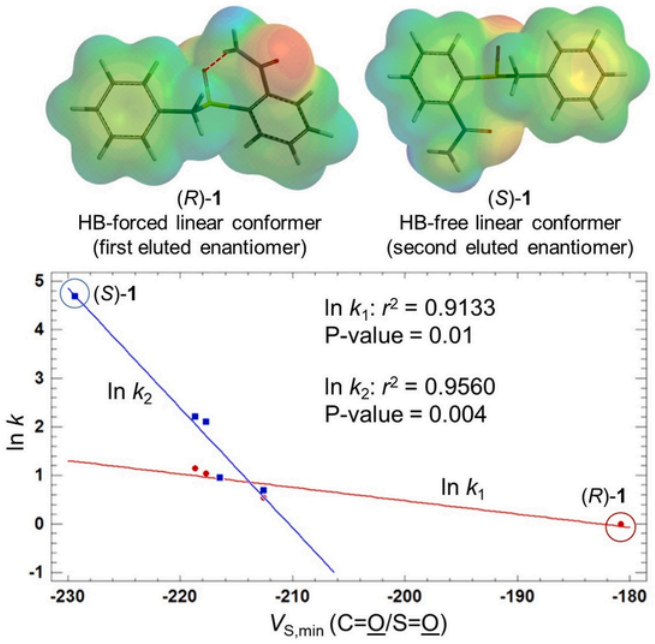

Sulfoxide (EEO)	ln k_1 = $f(V_{S,min})$ ln k_1	$V_{S,min}$ (S=O)[a]	$V_{S,min}$ (C=O)[a]	ln k_2 = $f(V_{S,min})$ ln k_2	$V_{S,min}$ (S=O)[a]	$V_{S,min}$ (C=O)[a]	ln α
2 (+/-)	0.54	-212.6	--	0.69	-212.6	--	0.16
3 (+/-)	0.96	-216.5	--	0.96	-216.5	--	0
4 (-/+)	1.03	--	-217.7	2.19	--	-217.7	1.07
22 (+/-)	1.14	-225.5	--	2.22	-218.7	--	1.07
1 (+/-)	-0.01	-182.6	--	4.70	-229.4	--	4.71

[a] [kJ/mol]

Fig. 4. Linear regression analysis describing the relationships between ln k_1 and ln k_2 (**CS1**, MP = 2-propanol) [12] and $V_{S,min}$ values for compounds **1**–**4** and **22**.

tween its ionized functional groups, that limit its conformational freedom and weaken the association with the CSP, whereas (*R*)-carnosine presents higher conformational freedom and ability to form intermolecular contacts with the CSP [11].

In series **1**–**4**, and **22**, selectivity (ln α) correlates with ln k_2 (r^2 = 0.9622, P-value = 0.003) (Supplementary data, Fig. S3a). On the contrary, a scatter plot was observed for ln α vs. ln k_1 (P-value = 0.13). Therefore, selectivity correlates with the same $V_{S,min}$ data set of the regression line ln k_2 = f ($V_{S,min}$) with r^2 = 0.9336 and P-value = 0.007 (Supplementary data, Fig. S3b), this evidence showing the stereoselective significance of the HBs between analytes and CSs. A moderate correlation was found between ln k_2 and dipole moment values of conformers $\mathbf{1}_{freeNH2\_linear}$, **2**, **3**, $\mathbf{4}_{HB}$, and $\mathbf{22}_C$ (r^2 = 0.8286, P-value = 0.03) (Supplementary data, Fig. S3c). On the contrary, no correlation was found between ln α and the same set of dipole moment values (P-value = 0.09), this fact suggesting that dipole moment controls nonstereoselective interactions related to retention of the second eluted enantiomer.

3.3. Impact of structural and conformational variations on enantioseparation

In light of the conformationally-driven mechanism determined for the enantioseparation of **1**, we calculated low-energy conformer distribution for compounds **5**–**9** (CH_2Ph→alkyl chain), **10** (2-benzylsulfinyl→3-benzylsulfinyl), **13** ($CONH_2$→COOMe), **14** ($CONH_2$→CONHMe), and **23** ($CONH_2$→COOH) which are related to **1** through subtle structural variations. On this basis, we aimed at exploring the relationship between enantioseparation extent and the presence of the pair HB-type/freeNH_2(NH)-type conformers. The results of the conformer distribution are summarized in Table 2, and a clear trend emerges for compounds **1**, **5**–**9** and **14** relating higher selectivity values, in the range 16–202.6 [25–27], to the pair of HB-type/freeNH_2(NH)-type conformers. Naturally, the extent of selectivity depends on the structural features of the corresponding sulfoxides. Otherwise, lower selectivity factors ranging from 1.2 to 2.83 are reported [25,27,29,30] *i)* for compounds **10**, which bear the NH_2 group far from the sulfinyl oxygen, and consequently no intramolecular HB can be formed, *ii)* for **13**, which are structurally unable to form intramolecular HB due to the lack of amidic hydrogens, and *iii)* for compounds **23**, in this case no HB-type conformer was found by calculation.

Table 2
Relative energies, and Boltzmann distribution for conformers of sulfoxides 1 (reference compound), 5–10, 13, 14, and 23 calculated through computational conformational search in vacuum (DFT/B3LYP/6-31G*) vs experimental selectivity factors (MP = 2-propanol or n-hexane-containing mixtures) [25–27].

sulfoxide conformer	ΔE [kcal/mol]	Boltzmann distribution	selectivity factor (α) (α (1) [a])
$\mathbf{1}_{HB\_bent}$	0	38.8	–
$\mathbf{1}_{HB\_linear}$	0.26	24.6	
$\mathbf{1}_{freeNH2\_linear}$	0.35	21.3	
$\mathbf{1}_{freeNH2\_bent}$	0.57	14.7	
$\mathbf{5}_{A\_HB}$	0	68.3	85 (150) [Ref. [26]]
$\mathbf{5}_{B\_HB}$	0.86	16.1	
$\mathbf{5}_{C\_freeNH2}$	0.92	14.4	
$\mathbf{5}_{D\_freeNH2}$	2.49	1.0	
$\mathbf{6}_{A\_HB}$	0	27.9	45 (150) [Ref. [26]]
$\mathbf{6}_{B\_HB}$	0.43	13.4	
$\mathbf{6}_{C\_HB}$	0.46	12.8	
$\mathbf{6}_{D\_freeNH2}$	0.84	6.6	
$\mathbf{7}_{A\_HB}$	0	38.7	26 (150) [Ref. [26]]
$\mathbf{7}_{B\_HB}$	0.39	19.2	
$\mathbf{7}_{C\_HB}$	0.54	14.6	
$\mathbf{7}_{D\_freeNH2}$	0.86	8.6	
$\mathbf{8}_{A\_HB}$	0	54.6	22 (150) [Ref. [26]]
$\mathbf{8}_{B\_HB}$	0.45	25.6	
$\mathbf{8}_{C\_freeNH2}$	0.86	13.0	
$\mathbf{9}_{A\_HB\ B}$	0	88.7	16 (150) [Ref. [26]]
$\mathbf{9}_{B\_freeNH2}$	0.86	10.3	
$\mathbf{10}_{A}$	0	66.8	1.2 (202.6) [Ref. [27]]
$\mathbf{10}_{B}$	1.73	33.2	
$\mathbf{13}_{A}$	0	57.9	1.82 (43) [Ref. [25]]
$\mathbf{13}_{B}$	0.26	37.4	
$\mathbf{13}_{C}$	1.79	2.8	
$\mathbf{13}_{D}$	2.11	1.6	
$\mathbf{14}_{HB\_bent}$	0	42.5	10 (43) [Ref. [25]] 24.3 (202.6) [Ref. [27]]
$\mathbf{14}_{freeNH\_linear}$	0.24	16.7	
$\mathbf{14}_{HB\_linear}$	0.13	28.0	
$\mathbf{14}_{freeNH\_bent}$	0.40	10.6	
$\mathbf{23}_{A}$	0	56.5	2.83 (43) [Ref. [25]]
$\mathbf{23}_{B}$	0.22	39.8	

[a] Selectivity observed for the enantioseparation of **1** under the same chromatographic conditions.

In methanol, selectivity of **1** and analogs decrease drastically compared to the enantioseparations performed with 2-propanol, or under normal phase conditions [27,29]. Indeed, inter- and intramolecular HB formation is expected to be disfavoured when methanol is used as MP. However, previous chromatographic studies provided strong evidences that HBs may be involved in the enantiodiscrimination of chiral sulfoxides with cellulose phenylcarbamate-based CSs even in pure methanol and in aqueous methanol with low content of water [29]. On this basis, we evaluated the conformer distribution of sulfoxides **1** and **10**–**21** in methanol (Supplementary data, Table S2) in order to explore a possible relationship between the pair of HB-type/freeNH_2(NH)-type conformers and higher selectivity values also in polar medium. In Table 3, the enantioseparations of compounds **1** and **10**–**21** on **CS1**-**CS17** with methanol 100% [29] are summarized and ranked in terms of rate% of enantioseparations obtained with $\alpha > 1$ and related α, as average value. Also in this case, compounds showing better selectivity (average $\alpha \geq 1.38$) are characterized by the pivotal conformer pair HB/freeNH_2(NH) in almost all cases, whereas compounds with lower selectivity (average $\alpha \leq 1.22$) do not present these conformational features.

Table 3
Conformer types (calculated with methanol as medium), rate (%) of enantioseparations with $\alpha > 1$ on CS1-CS17 with pure methanol as MP, and average α values ($\alpha > 1$) obtained for compounds 1, and 10–21. Experimental data from Ref. [29].

sulfoxide	conformer type	$\alpha > 1$ (%)	average α (>1)
1	HB/freeNH_2	94	5.17
11	noHB [a]	35	2.87
14	HB/freeNH	71	1.81
15	noHB [a]	76	1.79
20	HB/freeNH	76	1.63
19	HB/freeNH	53	1.53
21	HB/freeNH	76	1.48
18	HB/freeNH	65	1.38
13	noHB [a]	71	1.22
17	noHB [a]	23	1.24
12	noHB [a]	53	1.11
10	noHB [a]	12	1.10
16	noHB [a]	18	1.17

[a] For these sulfoxides no conformer containing intramolecular HB was found.

3.3.1. V_S analysis and enantiophoric systems

The calculation of V_S values and molecular properties for conformers of compounds **5**–**21** allowed to profile the corresponding enantiophore systems in terms of shape and electron charge density distribution (Supplementary data, Tables S4–S6). This information may shed light on the reason why subtle variations introduced in the lead structure (compound **1**) impact deeply the enantioseparation extent. Some representative cases are discussed below:

i) for compound **14** ($CONH_2$→CONHMe), lower selectivity was observed compared to **1** [27,29,30]. This decrease of selectivity is likely due to the lack of the second amidic proton, and to the steric hindrance exerted by the methyl group on close HB sites (Fig. 5). These structural factors profile different enantiophoric systems for **14** compared to **1**, in terms of site accessibility and electronic properties;
ii) for sulfoxide **10** (2-benzylsulfinyl→3-benzylsulfinyl), the key sites defining the enantiophoric system are located more or less on the same plane (Supplementary data, Fig. S4a) and the two enantiomers are almost superimposable and, consequently, less distinguishable compared to **1.** This observation could rationalize low or absent enantioseparation observed for this compound on almost all CSs [27,29,30]. The same structural effect may be responsible of the poor enantioseparations observed for **16** [29]. The corresponding enantiophore again presents the HB sites located more or less in

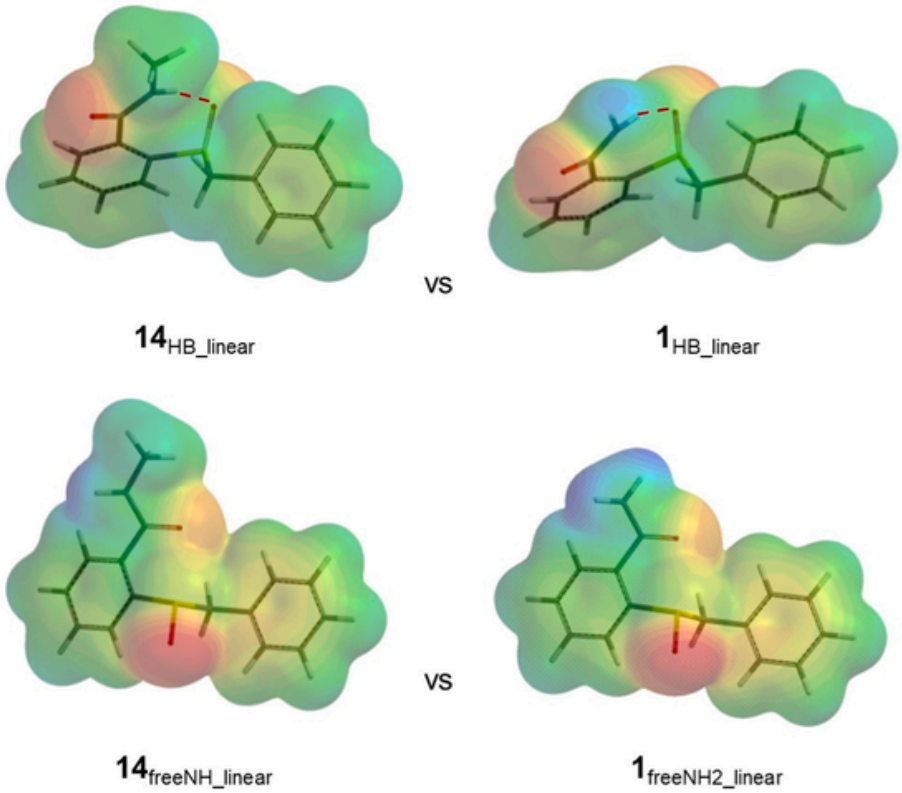

Fig. 5. Comparison of compounds **1** and **14** profiled by V_S representation on isodensity isosurfaces identifying distinctive enantiophoric systems.

the same plane (Fig. S4b), this kind of assembly limiting the discriminability of the enantiomer pair;

iii) on the other hand, for **10** higher retention of the first eluted enantiomer is reported compared to **1** [27,29]. This trend may be rationalized on the basis of the electronic properties of the respective HB sites. Indeed, the HB donor ability of the main amidic proton of **10** ($V_{S,max,vacuum}$ = 212.9 kJ/mol; $V_{S,max,methanol}$ = 278.6 kJ/mol) is higher compared to the first eluted conformer of **1** (HB-type) ($V_{S,max,vacuum}$ = 168.2 kJ/mol; $V_{S,max,methanol}$ = 168.2 kJ/mol). In addition, also the HB acceptor ability of the sulfinyl oxygen of **10** ($V_{S,min,vacuum}$ = −196.6 kJ/mol; $V_{S,min,methanol}$ = −267.8) is higher compared to $\mathbf{1}_{HB\text{-}type}$ conformer ($V_{S,min,vacuum}$ = −182.6 kJ/mol; $V_{S,min,methanol}$ = −210.3).

3.4. Cellulose tris(3,5-dichlorophenylcarbamate) vs cellulose tris(3,5-dimethylphenylcarbamate): impact of chlorination

Comparing enantioseparations of **1** on **CS1** and **CS2**, the ratio $\alpha_{CS1}/\alpha_{CS2}$ is 6 in methanol [29] and increase to 42 in 2-propanol [12]. In cellulose carbamate-based CSs, the substituents on the phenyl ring impact significantly the capability of N–H and C=O groups of the carbamate moiety as HB donor and acceptor, respectively. Moreover, the SC moiety can also promote dipole-dipole, π-π interactions and hydrophobic contacts. On this basis, the V_S associated to **SC1** and **SC2** regions was inspected with the aim to explain the chromatographic trend. As shown in Fig. 6, the V_S values associated with the N–H and the C=O sites are positive and negative, respectively, according with the function of the amidic hydrogen as HB donor, and the carbonyl oxygen as HB acceptor. Comparing the V_S values of the 3,5-dimethylated **SC2** and the 3,5-dichlorinated **SC1** calculated in the vacuum, it can be observed that chlorination causes a decrease of the C=O capability as HB acceptor, with a reduced electron charge density on the oxygen ($V_{S,min}$ decreases from −169.9 to −144.3 kJ/mol), and an increase of the N–H capability as HB donor due to the decrease of electron charge density on the hydrogen ($V_{S,max}$ increases from 201.4 to 246.2 kJ/mol). This effect has consequence at intermolecular level for the interaction analyte-CS as well as at intramolecular level, affecting the formation of intramolecular HBs in CS which contribute to maintain the high-ordered structure of the CS. In this regard, it was observed through IR analyses that the introduction of chlorine increases the fraction of free N–H groups available for intermolecular HBs [4,49]. In the meantime, the fraction of N–H involved in intramolecular HBs decreases. This could produce for the chlorinated **CS1** a wider cavity available for the enantiomers with respect to the cellulose *tris*(3,5-dimethylphenylcarbamate) (CDMPC) (**CS2**), the enantioseparation resulting from the balance of carbamate polarity and intramolecular HB ability [4,49]. Coherently, a less negative V_S value was calculated for the π-cloud of the chlorinated phenyl ring of **SC1** ($V_{S,min}$ = −39.1 kJ/mol) compared to the 3,5-dimethylated phenyl ring of **SC2** ($V_{S,min}$ = −94.6 kJ/mol). Moreover, the chlorinated **SC1** shows lower values of molecular area and volume than **SC2**. Taking into account the chromatographic trend, it is clear that the **SC1** landscape in term of V_s pattern is more suitable for the enantioseparation of **1** compared to the **SC2**, suggesting a pivotal role of HBs between the carbamate N–H of the CS as HB donor and the regions with high electron charge density of the chiral sulfoxide as HB acceptors.

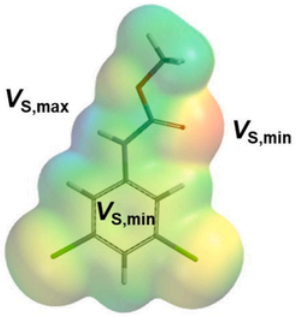

methyl
(3,5-dichlorophenylcarbamate)
(**SC1**)

SC	$V_{S,min}$[a] (C=O)	$V_{S,min}$[a] (Ar)	$V_{S,max}$[a] (N-H)	Area[b]	Volume[c]	α[d]
SC1	-144.3	-39.1	246.2	210.8	192.9	10.27
SC2	-169.9	-94.6	201.4	214.7	195.9	1.62

[a] V_S [kJ/mol]; [b] Isosurface area [Å^2]; [c] Volume enclosed in the isosurface [Å^3]; [d] Selectivity values for the enantioseparation of **1** on **CS1** and **CS2**, from ref. [29].

Fig. 6. V_S representation on electron density isosurfaces of methyl (3,5-dichlorophenylcarbamate) **SC1** as model of the distinctive side chain of cellulose *tris*(3,5-dichlorophenylcarbamate) (**CS1**). V_S values, area and volume of the isosurfaces, calculated in the vacuum are reported for **SC1** and methyl (3,5-dimethylphenylcarbamate) **SC2**. Experimental values of α are reported from Refs. [29].

3.4.1. Enantioseparation capability of cellulose-based chiral selectors toward 1

Given the previous analysis, the dependence of retention and selectivity factors on calculated molecular properties of the models **SC1**-**SC17** was explored, referring to the benchmark enantioseparations of **1** on **CS1**-**CS17** with methanol as MP (Supplementary data, Table S7) [29]. Therefore, we computed V_S values for **SC1**-**SC17** using methanol as virtual solvent and focusing on amidic hydrogen N–H ($V_{S,max}$), the carbonyl oxygen C=O ($V_{S,min}$) and the π-cloud of the aromatic ring ($V_{S,min}$). For each SC other properties, such as area and volume of the isosurface, log P and dipole moment were also computed (see Supplementary data, Fig. S5, Tables S8 and S9). The series of SCs contains monochlorinated (**SC3**, **SC4**, **SC5**), monomethylated (**SC11**, **SC12**, **SC13**), dichlorinated (**SC1**, **SC4**, **SC6**, **SC7**, **SC8**, **SC9**, **SC10**), dimethylated (**SC2**, **SC14**), chloromethylated (**SC15**, **SC16**) and unsubstituted (**SC17**) phenylcarbamates (Table 1). As reported in Fig. 7, retention values of the first eluted enantiomer do no correlate with selectivity and a scatter plot is observed (Fig. 7a), whereas selectivity values correlate with the retention values of the second elute enantiomer (r^2 = 0.9556, P-value = 0.000) (Fig. 7b). The retention values of both enantiomers correlate (moderately for ln k_1 and strongly for ln k_2) (Fig. 7c) with the electron charge density of the amidic hydrogen of the CSs which is expressed in terms of $V_{S,max}$ values calculated on the amidic hydrogen regions. Otherwise, the other calculated molecular properties furnished no statistically significant correlation, showing P-values > 0.05 in all cases. However, some trends could be observed. Indeed, ln k_2 showed to increase as the electron charge density on the carbonyl oxygens (Fig. 7d) and the dipole moment (Fig. 7e) decreases and increases, respectively. Otherwise, ln k_1 appears unaffected by both dipole moment and $V_{S,min}$ calculated on the carbonyl oxygens. On this basis, a model using the electron charge density on the main sites of the carbamate regions, as independent variables, shows to describe well the enantioseparations of fifteen CSs (r^2 = 0.8532, P-value = 0.0000) (Fig. 7f), whereas the introduction of **CS15** and **CS16** in the series lowers both r^2 and P-values, even if the correlation still saves its statistical significance (r^2 = 0.6654, P-value = 0.0002). This observation suggests that additional effects control the enantioseparations in **CS15** and **CS16**, likely in terms of ability to exert dipole-dipole interactions and HBs as acceptor, producing higher selectivity toward **1** (α = 15.97 and 19.82, respectively). In this regard, it is worth noting that in **CS1**-**CS14** chlorines and methyl groups on the aromatic ring modify the electron charge density on carbonyl oxygens and amidic protons in a complementary manner, increasing or decreasing the electron charge density on one site and decreasing or increasing, respec-

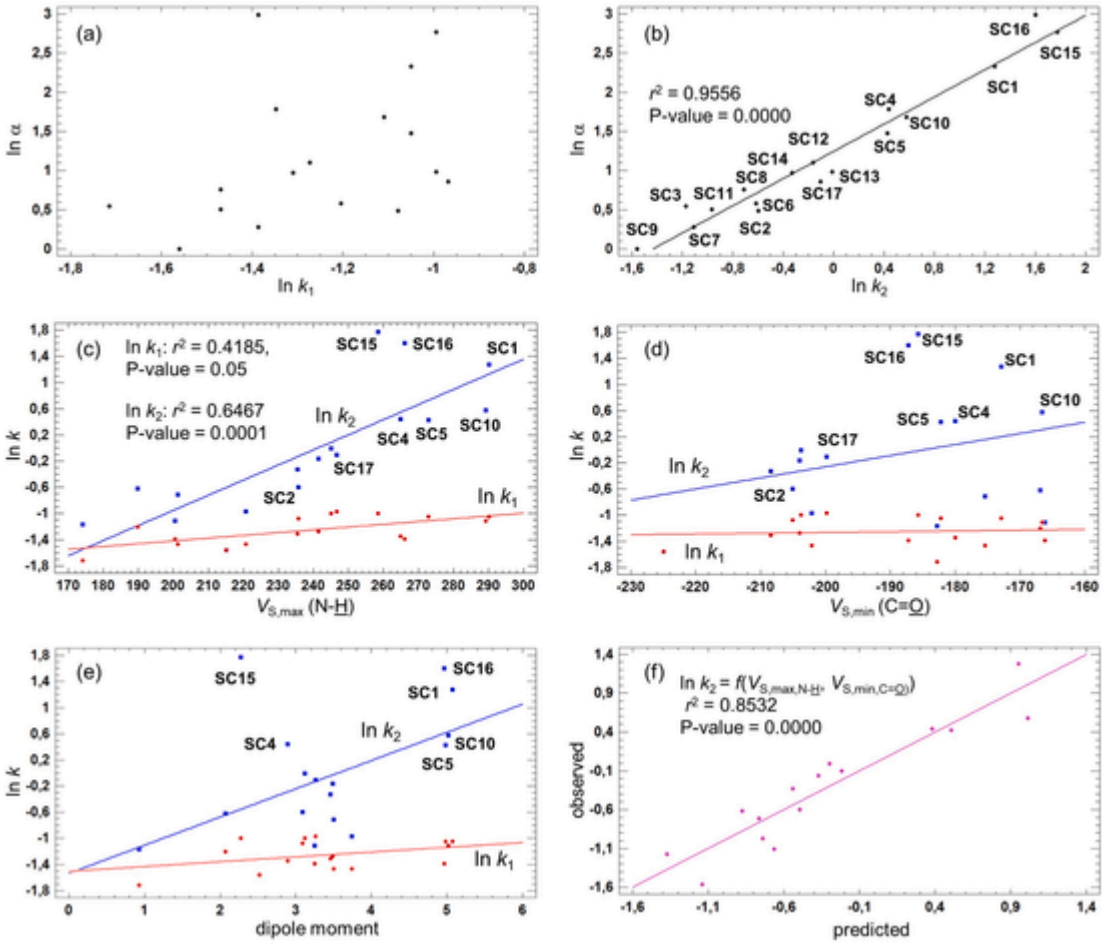

Fig. 7. Linear regression analysis describing for **1** the relationships between ln k_1 and ln k_2 (**CS1-CS17**, MP = methanol) [29] and molecular properties of **SC1-SC17**.

tively, the electron charge density on the other site. Otherwise, **CS15** and **CS16** show high and low electron charge density on carbonyl oxygens and the amidic hydrogens, respectively, which are both as high as possible due to suitable electronic effects exerted by chlorine and methyl as substituents at position 3 and 4 of the aromatic ring.

4. Conclusions

The computational procedure presented herein allowed for profiling a recognition model to describe the exceptional selectivity of **1** on cellulose-based CSs, explaining several aspects impacting enantioseparation as subtle modifications are introduced in the lead structure. Indeed, computational results and correlations between computed and benchmark experimental data support the following trends: *i)* features and electronic properties of low-energy conformers calculated for each sulfoxide profile the enantiophoric system potentially occurring on the surface of the CS during the enantiodiscrimination process; *ii)* for **1** and related derivatives bearing either the amidic NH_2 or NH groups, low-energy conformers containing an intramolecular HB between the sulfinyl oxygen and amidic proton were identified. Chiral sulfoxide bearing this feature are in general recognized better; *iii)* a conformational transition between low-energy conformers associated with distinct enantiophoric systems for the first and the second eluted enantiomer, respectively, can reasonably explain the exceptional enantioseparation of **1** on chlorinated cellulose carbamate-based CSs; *iv)* the main interaction driving enantioseparations of **1** on seventeen chlorinated cellulose-based CS is the HB between the sulfinyl oxygen of the analyte and the amidic hydrogen of the selector, whereas the participation of the carbamate oxygen determines exceptional enantioseparations only for **CS15** and **CS16**. In fact, in terms of electronic properties, these CSs contain carbamates moieties with both HB donor and acceptor abilities as high as possible compared to the other CSs examined in this study.

Given that, three types of HB contacts appear to be of crucial importance for the enantioseparation of chiral sulfoxides on cellulose carbamate-based CSs: *i)* intramolecular HBs within the polysaccharide derivative, contributing to sustain the high-ordered structure of the polymeric selector. The strength of these intramolecular HBs depends on steric and electronic properties of each distinctive SC, also determining chiral cavity size and shape; *ii)* as demonstrated in this study, stereoselective intramolecular HBs within the analyte may have a pivotal role in enantiodifferentiation, limiting conformational freedom of a single enantiomer and weakening its ability to exert intermolecular HBs with the CS, and defining different enantiophore systems for each eluted enantiomer; *iii)* intermolecular HBs between analyte and selector sustaining diastereomeric complex formation and discrimination.

Importantly, conformational and electrostatic potential analysis may be applicable to other chromatographic systems providing a rationale of why and how the analytical separation occurs.

CRediT authorship contribution statement

Paola Peluso: Conceptualization, Data curation, Formal analysis, Investigation, Methodology, Writing - original draft, Writing - review & editing. **Bezhan Chankvetadze:** Conceptualization, Project administration, Writing - review & editing.

Declaration of competing interest

The authors declare that they have no known competing financial interests or personal relationships that could have appeared to influence the work reported in this paper.

Appendix A. Supplementary data

Supplementary data to this article can be found online at https://doi.org/10.1016/j.aca.2020.10.050.

References

[1] N.M. Maier, P. Franco, W. Lindner, Separation of enantiomers: needs, challenges, perspectives, J. Chromatogr. A 906 (2001) 3–33.

[2] K.K. Unger, R. Ditz, E. Machtejevas, R. Skudas, Liquid chromatography - its development and key role in life science applications, Angew. Chem. Int. Ed. 49 (2010) 2300–2312.

[3] K. Si-Ahmed, Z. Aturki, B. Chankvetadze, S. Fanali, Evaluation of novel amylose and cellulose-based chiral stationary phases for the stereoisomer separation of flavanones by means of nano-liquid chromatography, Anal. Chim. Acta 738 (2012) 85–94.

[4] B. Chankvetadze, Polysaccharide-based chiral stationary phases for enantioseparations by high-performance liquid chromatography: an overview, in: G.K.E. Scriba (Ed.), Chiral Separations: Methods and Protocols, Methods in Molecular Biology, 1985, Springer Science + Business Media, LLC, part of Springer Nature, 2019, pp. 93–126.

[5] G.K.E. Scriba, Chiral recognition in separation science – an update, J. Chromatogr. A 1467 (2016) 56–78.

[6] P. Peluso, V. Mamane, R. Dallocchio, A. Dessì, S. Cossu, Noncovalent interactions in high-performance liquid chromatography enantioseparations on polysaccharide-based chiral selectors, J. Chromatogr. A 1623 (2020) 461202.

[7] P. Peluso, A. Dessì, R. Dallocchio, V. Mamane, S. Cossu, Recent studies of docking and molecular dynamics simulation for liquid-phase enantioseparations, Electrophoresis 40 (2019) 1881–1896.

[8] R. Sardella, E. Camaioni, A. Macchiarulo, A. Gioiello, M. Marinozzi, A. Carotti, Computational studies in enantioselective liquid chromatography: forty years of evolution in docking- and molecular dynamics-based simulations, Trends Anal. Chem. 122 (2020) 115703.

[9] T.D. Booth, I.W. Wainer, Investigation of the enantioselective separations of α-alkylarylcarboxylic acids on an amylose tris(3,5-dimethylphenylcarbamate) chiral stationary phase using quantitative structure-enantioselective retention relationships. Identification of a conformationally driven chiral recognition mechanism, J. Chromatogr. A 737 (1996) 157–169.

[10] T.D. Booth, I.W. Wainer, Mechanistic investigation into the enantioselective separation of mexiletine and related compounds, chromatographed on an amylose tris(3,5-dimethylphenylcarbamate) chiral stationary phase, J. Chromatogr. A 741 (1996) 205–211.

[11] R. Sardella, F. Ianni, L. Cossignani, G. Aldini, A. Carotti, Binding modes identification through molecular dynamic simulations: a case study with carnosine enantiomers and the Teicoplanin A2-2-based chiral stationary phase, J. Separ. Sci. 43 (2020) 1728–1736.

[12] B. Chankvetadze, C. Yamamoto, Y. Okamoto, Enantioseparation of selected chiral sulfoxides using polysaccharide-type chiral stationary phases and polar organic, polar aqueous-organic and normal-phase eluents, J. Chromatogr. A 922 (2001) 127–137.

[13] R. Cirilli, S. Alcaro, R. Fioravanti, R. Ferretti, A. Bolasco, B. Gallinella, C. Faggi, A chromatographic study on the exceptional enantioselectivity of cellulose tris(4-methylbenzoate) towards C5-chiral 4,5-dihydro-(1H)-pyrazole derivatives, J. Chromatogr. A 1218 (2011) 5653–5657.

[14] S. Alcaro, A. Bolasco, R. Cirilli, R. Ferretti, R. Fioravanti, F. Ortuso, Computer-aided molecular design of asymmetric pyrazole derivatives with exceptional enantioselective recognition toward the Chiralcel OJ-H stationary phase, J. Chem. Inf. Model. 52 (2012) 649–654.

[15] P. Peluso, V. Mamane, E. Aubert, S. Cossu, Optimization of the HPLC enantioseparation of 3,3'-dibromo-5,5'-disubstituted-4,4'-bipyridines using immobilized polysaccharide-based chiral stationary phases, J. Separ. Sci. 36 (2013) 2993–3003.

[16] E. Kiisters, V. Loux, E. Schmid, Enantiomeric separation of chiral sulphoxides. Screening of cellulose-based sorbents with particular reference to cellulose tribenzoate, J. Chromatogr. A 666 (1994) 421–432.

[17] S.A. Matlin, M.E. Tiritan, Q.B. Cass, D.R. Boyd, Enantiomeric resolution of chiral sulfoxides on polysaccharide phases by HPLC, Chirality (1996) 8147–8152.

[18] Q. Cass, F. Batigalhia, Enantiomeric resolution of a series of chiral sulfoxides by high-performance liquid chromatography on polysaccharide-based columns with multimodal elution, J. Chromatogr. A 987 (2003) 445–452.

[19] S. Materazzo, S. Carradori, R. Ferretti, B. Gallinella, D. Secci, R. Cirilli, Effect of the water content on the retention and enantioselectivity of albendazole and fenbendazole sulfoxides using amylose-based chiral stationary phases in organic–aqueous conditions, J. Chromatogr. A 1327 (2014) 73–79.

[20] M. Gegenava, L. Chankvetadze, T. Farkas, B. Chankvetadze, Enantioseparation of selected chiral sulfoxides in high-performance liquid chromatography with polysaccharide-based chiral selectors in polar organic mobile phases with emphasis on enantiomer elution order, J. Separ. Sci. 37 (2014) 1083–1088.

[21] N. Kolderová, T. Neveselý, J. Šturala, M. Kuchař, R. Holakovský, M. Kohout, Enantioseparation of chiral sulfoxides on amylose-based columns: comparison of normal phase liquid chromatography and supercritical fluid chromatography, Chromatographia 80 (2017) 547–557.

[22] A. Panusa, A. Rosetti, C. Villani, R. Cirilli, Direct HPLC enantioseparation of chemopreventive chiral isothiocyanates sulforaphane and iberin on immobilized amylose-based chiral stationary phases under normal-phase, polar organic and aqueous conditions, Talanta 218 (2020) 121151.

[23] R. Sardella, F. Ianni, A. Di Michele, A. Di Capua, A. Carotti, M. Anzini, B. Natalini, Enantioresolution and stereochemical characterization of two chiral sulfoxides endowed with COX-2 inhibitory activity, Chirality 29 (2017) 536–540.

[24] B. Chankvetadze, C. Yamamoto, Y. Okamoto, Extremely high enantiomer recognition in HPLC separation of racemic 2-(benzylsulfinyl)benzamide using cellulose tris(3,5-dichlorophenylcarbamate) as a chiral stationary phase, Chem. Lett. (2000) 1176–1177.

[25] S. Carradori, D. Secci, C. Faggi, R. Cirilli, A chromatographic study on the exceptional chiral recognition of 2-(benzylsulfinyl)benzamide by an immobilized-type chiral stationary phase based on cellulose tris(3,5-dichlorophenylcarbamate), J. Chromatogr. A 1531 (2018) 151–156.

[26] S. Carradori, D. Secci, P. Guglielmi, M. Pierini, R. Cirilli, High-performance liquid chromatography enantioseparation of chiral 2-(benzylsulfinyl)benzamide derivatives on cellulose tris(3,5-dichlorophenylcarbamate) chiral stationary phase, J. Chromatogr. A 1610 (2020) 460572.

[27] T. Khatiashvili, R. Kakava, I. Matarashvili, H. Tabani, C. Fanali, A. Volonterio, T. Farkas, B. Chankvetadze, Separation of enantiomers of selected chiral sulfoxides with cellulose tris(4-chloro-3-methylphenylcarbamate)-based chiral columns in high-performance liquid chromatography with very high separation factor, J. Chromatogr. A 1545 (2018) 59–66.

[28] N. Khundadze, S. Pantsulaia, C. Fanali, T. Farkas, B. Chankvetadze, On our way to sub-second separations of enantiomers in high-performance liquid chromatography, J. Chromatogr. A 1572 (2018) 37–43.

[29] Z. Shedania, R. Kakava, A. Volonterio, T. Farkas, B. Chankvetadze, Separation of enantiomers of chiral sulfoxides in high-performance liquid chromatography with cellulose-based chiral selectors using methanol and methanol-water mixtures as mobile phases, J. Chromatogr. A 1557 (2018) 62–74.

[30] Z. Shedania, R. Kakava, A. Volonterio, T. Farkas, B. Chankvetadze, Separation of enantiomers of chiral sulfoxides in high-performance liquid chromatography with cellulose-based chiral selectors using acetonitrile and acetonitrile-water mixtures as mobile phases, J. Chromatogr. A 1609 (2020) 460445.

[31] S. Pantsulaia, K. Targamadze, N. Khundadze, Q. Kharaishvili, A. Volonterio, M. Chity, T. Farkas, B. Chankvetadze, Potential and current limitations of superficially porous silica as a carrier for polysaccharide-based chiral selectors in separation of enantiomers in high-performance liquid-chromatography, J. Chromatogr. A 1625 (2020) 461297.

[32] B. Chankvetadze, Recent trends in preparation, investigation and application of polysaccharide-based chiral stationary phases for separation of enantiomers in high-performance liquid chromatography, Trends Anal. Chem. 122 (2020) 115709.

[33] C. West, M.–L. Konjaria, N. Shashviashvili, E. Lemasson, P. Bonnet, R. Kakava, A. Volonterio, B. Chankvetadze, Enantioseparation of novel chiral sulfoxides on chlorinated polysaccharide stationary phases in supercritical fluid chromatography, J. Chromatogr. A 1499 (2017) 174–182.

[34] S. Felletti, C. De Luca, G. Lievore, T. Chenet, B. Chankvetadze, T. Farkas, A. Cavazzini, M. Catani, Shedding light on mechanisms leading to convex-upward van Deemter curves on a cellulose tris(4-chloro-3-methylphenylcarbamate)-base chiral stationary phase, J. Chromatogr. A 1630 (2020) 461532.

[35] M.L.C. Montanari, Q.B. Cass, A. Leitão, A.D. Andricopulo, C.A. Montanari, The role of molecular interaction field on enantioselective and nonselective separation of chiral sulfoxides, J. Chromatogr. A 1121 (2006) 64–75.

[36] F. Xiong, B.–B. Yang, J. Zhang, L. Li, Enantioseparation, stereochemical assignment and chiral recognition mechanism of sulfoxide-containing drugs, Molecules 23 (2018) 2680.

[37] Y. Shao, L.F. Molnar, Y. Jung, J. Kussmann, C. Ochsenfeld, S.T. Brown, A.T.B. Gilbert, L.V. Slipchenko, S.V. Levchenko, D.P. O'Neil, R.A. Di Stasio Jr., R.C. Lochan, T. Wang, G.J.O. Beran, N.A. Besley, J.M. Herbert, C.Y. Lin, T. Van Voorhis, S. H Chien, A. Sodt, R.P. Steele, V.A. Rassolov, P.E. Maslen, P.P. Korambath, R.D. Adamson, B. Austin, J. Baker, E.F.C. Byrd, H. Dachsel, R.J. Doerksen, A. Dreuw, B.D. Dunietz, A.D. Dutoi, T.R. Furlani, S.R. Gwaltney, A. Heyden, S. Hirata, C.-P. Hsu, G. Kedziora, R.Z. Khalliulin, P. Klunzinger, A.M. Lee, M.S. Lee, W.Z. Liang, I. Lotan, N. Nair, B. Peters, E.I. Proynov, P.A. Pieniazek, Y.M. Rhee, J. Ritchie, E. Rosta, C.D. Sherrill, A.C. Simmonett, J.E. Subotnik, H.L. Woodcock III, W. Zhang, A.T. Bell, A.K. Chakraborty, D.M. Chipman, F.J. Keil, A. Warshel, W.J. Hehre, H.F. Schaefer, J. Kong, A.I. Krylov, P.M.W. Gill, M. Head-Gordon, Advances in methods and algorithms in a modern quantum chemistry program package, Phys. Chem. Chem. Phys. 8 (2006) 3172–3191.

[38] C.C. Chambers, G.D. Hawkins, C.J. Cramer, D.G. Truhlar, Model for aqueous solvation based on class IV atomic charges and first solvation shell effects, J. Phys. Chem. 100 (1996) 16385–16398.

[39] A.V. Marenich, R.M. Olsen, C.P. Kelly, C.J. Cramer, D.G. Truhlar, Self-consistent reaction field model for aqueous and nonaqueous solutions based on accurate polarized partial charges, J. Chem. Theor. Comput. 3 (2007) 2011–2033.
[40] J.S. Murray, P. Politzer, Molecular electrostatic potentials and noncovalent interactions, WIREs Comput, Mol. Sci. 7 (2017) e1326.
[41] B.-H. Kim, S.U. Lee, D.C. Moon, Chiral recognition of N-phthaloyl, N-tetrachlorophthaloyl, and N-naphthaloyl α-amino acids and their esters on polysaccharide-derived chiral stationary phases, Chirality 24 (2012) 1037–1046.
[42] P. Peluso, S. Cossu, Comparative HPLC enantioseparation of thirty-six aromatic compounds on four columns of the Lux series: impact of substituents, shapes and electronic properties, Chirality 25 (2013) 709–718.
[43] P. Peluso, V. Mamane, E. Aubert, A. Dessì, R. Dallocchio, A. Dore, P. Pale, S. Cossu, Insights into halogen bond-driven enantioseparations, J. Chromatogr. A 1467 (2016) 228–238.
[44] A. Del Rio, P. Piras, C. Roussel, Enantiophore modeling in 3D-QSAR. A data mining application on Whelk-O1 chiral stationary phase, Chirality 18 (2006) 498–508.
[45] S. Mecozzi, A.P. West Jr., D.A. Dougherty, Cation-π interactions in aromatics of biological and medicinal interest: electrostatic potential surfaces as a useful qualitative guide, Proc. Natl. Acad. Sci. U.S.A. 93 (1996) 10566–10571.
[46] T. Clark, Halogen bonds and σ-holes, Faraday Discuss 203 (2017) 9–27.
[47] K.E. Riley, K.-.A. Tran, P. Lane, J.S. Murray, P. Politzer, Comparative analysis of electrostatic potential maxima and minima on molecular surfaces, as determined by three methods and a variety of basis sets, J. Comput. Sci. 17 (2016) 273–284.
[48] M.D. Perera, J. Desper, A.S. Sinha, C.B. Aakeröy, Impact and importance of electrostatic potential calculations for predicting structural patterns of hydrogen and halogen bonding, CrystEngComm 18 (2016) 8631–8636.
[49] B. Chankvetadze, L. Chankvetadze, S. Sidamonidze, E. Kasashima, E. Yashima, Y. Okamoto, 3-Fluoro-, 3-chloro- and 3-bromo-5-methylphenylcarbamates of cellulose and amylose as chiral stationary phases for high performance liquid chromatographic enantioseparation, J. Chromatogr. A 787 (1997) 67–77.